HHS Public Access

Author manuscript

Mol Cancer Ther. Author manuscript; available in PMC 2022 August 01.

Published in final edited form as:

Mol Cancer Ther. 2022 February ; 21(2): 322–335. doi:10.1158/1535-7163.MCT-21-0344.

Combination of type I and type II MET tyrosine kinase inhibitors as therapeutic approach to prevent resistance

Magda Bahcall[1], **Cloud P. Paweletz**[2], **Yanan Kuang**[2], **Luke J. Taus**[2], **Taebo Sim**[3,4], **Nam Doo Kim**[5], **Kshiti H. Dholakia**[1], **Christie J. Lau**[2], **Prafulla C. Gokhale**[2], **Pratik R. Chopade**[2], **Fangxin Hong**[6,7], **Zihan Wei**[6], **Jens Köhler**[1], **Paul T. Kirschmeier**[2], **Jiannan Guo**[8], **Sujuan Guo**[2], **Stephen Wang**[2], **Pasi A. Jänne**[1,2,9,*]

[1]Lowe Center for Thoracic Oncology, Dana-Farber Cancer Institute, Boston, MA

[2]Belfer Center for Applied Cancer Science, Dana-Farber Cancer Institute, Boston, MA

[3]Severance Biomedical Science Institute, Yonsei University College of Medicine, Seoul, South Korea

[4]Graduate School of Medical Science, Brain Korea 21 Project, Yonsei University College of Medicine, Seoul, South Korea

[5]VORONOI BIO Inc., Incheon, Republic of Korea

[6]Department of Data Science, Dana-Farber Cancer Institute, Boston, MA

[7]Harvard T.H. Chan School of Public Health, Boston, MA

[8]Resolution Bioscience, Kirkland, WA

[9]Department of Medicine, Brigham and Women's Hospital and Harvard Medical School, Boston, MA

Abstract

MET targeted therapies are clinically effective in *MET* amplified and *MET* exon 14 deletion mutant (*MET*ex14) non-small cell lung cancers (NSCLC) but their efficacy is limited by the development of drug resistance. Structurally distinct MET tyrosine kinase inhibitors (TKIs) (type I/II) have been developed or are under clinical evaluation, which may overcome *MET* mediated drug resistance mechanisms. In this study, we assess secondary MET mutations likely to emerge in response to treatment with single-agent or combinations of type I/type II MET TKIs using TPR-MET transformed Ba/F3 cell mutagenesis assays. We found that these inhibitors gave rise

[*]Corresponding author: Pasi A. Jänne, MD PhD, 450 Brookline Ave; LC4114, Boston, MA 02215, Phone: 617-632-6036, pasi_janne@dfci.harvard.edu.

Conflicts of Interest:

P.A.J. has received consulting fees from AstraZeneca, Boehringer-Ingelheim, Pfizer, Roche/Genentech, Takeda Oncology, ACEA Biosciences, Eli Lilly and Company, Araxes Pharma, Ignyta, Mirati Therapeutics, Novartis, LOXO Oncology, Daiichi Sankyo, Sanofi Oncology, Voronoi, SFJ Pharmaceuticals, Biocartis, Novartis Oncology, Nuvalent, Esai, Bayer, Transcenta ,Silicon Therapeutics, Allorion Therapeutics, Accutar Biotech and AbbVie; receives post-marketing royalties from DFCI owned intellectual property on EGFR mutations licensed to Lab Corp; receives or has received sponsored research funding from AstraZeneca, Astellas, Daichi-Sankyo, PUMA, Boehringer Ingelheim, Eli Lilly and Company, Revolution Medicines, and Takeda; and has stock ownership in Gatekeeper Pharmaceuticals. J.G. is an employee of Resolution Bioscience and has stock-based incentive.
All other authors declare no conflicts of interest.

to distinct secondary MET mutant profiles. However, a combination of type I/II TKI inhibitors (capmatinib and merestinib) yielded no resistant clones *in vitro*. The combination of capmatinib/merestinib was evaluated *in vivo* and led to a significant reduction in tumor outgrowth compared to either MET inhibitor alone. Our findings demonstrate *in vitro* and *in vivo* that a simultaneous treatment with a type I and type II MET TKI may be a clinically viable approach to delay and/or diminish the emergence of on target MET mediated drug resistance mutations.

Keywords

Lung cancer; drug resistance; mutation; MET proto-oncogene; receptor tyrosine kinase

Introduction

MET encodes the tyrosine kinase proto-oncogene MET, the receptor for hepatocyte growth factor (HGF). Exon 14 constituting the juxtamembrane domain of MET is the site of a number of negative regulatory residues and motifs critical for MET stability and/or tyrosine kinase activity (1). Mutations within those residues or the deletion of the entire exon 14 due to mutations in sites critical for correct MET splicing may consequently dysregulate these processes. Among those, the mutation or loss of the Tyr1003 residue prevents the binding of the E3 ubiquitin ligase Cbl, affording increased stability to MET (2,3); mutation or loss of Ser985, the site of inhibitory phosphorylation conferred by PKC, may render MET insensitive to signals muting its activation (4,5); mutation or loss of the ESVD motif, the site of caspase-mediated cleavage which abrogates ligand-induced signaling by separating the tyrosine kinase domain (TKD) from the extracellular domain, may result in prolonged activation of MET (6); mutation or loss of the proteolysis signal PEST sequence may further stabilize the MET protein (7).

Molecular profiling of 38028 tumor samples by targeted next-generation sequencing (NGS) highlighted the wide spectrum of MET exon 14 (*MET*ex14) alterations across a variety of cancer types, including lung, gastric, colorectal, and brain cancers (8). Among those, *MET*ex14 alterations have in particular stood out as relatively frequent oncogenic drivers in NSCLC (3-6% of all NSCLC), having since been validated as a biomarker of sensitivity to MET tyrosine kinase inhibitors (TKIs) (8-11) (Supplementary Table S1).

Despite dramatic responses seen in some *MET* amplified or *MET*ex14 mutant NSCLC patients treated with MET-directed TKIs, however, acquired resistance inevitably develops most commonly due to compensatory signaling (12-15), estimated as ~45% (16), or secondary mutations in the *MET* TKD (at ~30% incidence) (16), which constrain adequate binding of the drug to the kinase (16-20).

MET inhibitors fall into several functionally distinct classes based on their proclivity to bind to a particular activation state, domain and/or specific amino acid (aa) residues or pockets of MET (21-23). Type I inhibitors compete with ATP for binding to the ATP-binding pocket of the active, or *DFG-in*, conformation of MET. Type I inhibitors are further defined as type Ia or Ib based on their requirement for intact G1163, a residue analogous to G1202 in ALK and G2032 in ROS1 (23). Crizotinib, a type Ia inhibitor, interacts with G1163 and as such

is vulnerable to mutations in this residue. In contrast, the type 1Ib inhibitors capmatinib and savolitinib do not depend for binding on the G1163 residue. Type-II ATP-competitive MET kinase inhibitors are defined by their ability to trap MET in its inactive, or *DFG-out*, state, whereby they create and exploit an additional hydrophobic pocket adjacent to the MET ATP binding site. This feature provides type II inhibitors with certain advantages over their type I counterparts, namely in their potential for increased kinase specificity and slower off-rates (24). Examples of type II MET TKIs are the FDA-approved multi-kinase inhibitor cabozantinib, and glesatinib and merestinib currently in clinical development.

To date, a handful of studies have characterized mechanisms of resistance to MET TKIs attributable to the activation of compensatory parallel signaling pathways driven by wild type (WT) *KRAS* amplification (12,25), mutant *KRAS, BRAF* and *EGFR* (13,25), and proposed drug combination strategies to disrupt the signaling bypass. Several studies have also reported on resistance mechanisms associated with treatment-induced acquired secondary MET mutations and suggested alternative MET TKIs as next-line therapies for patients with disease progression (17,18,26). While this intuitive approach has proved to be successful in targeting acquired secondary MET mutations in the clinic and extending overall survival (18), it has left patients vulnerable to developing other secondary MET mutations that had been successfully targeted by TKIs administered in first-line. The concept of combining MET TKIs of distinct resistance profiles seems sensible to explore in order to address this issue and has not, to our knowledge, been proposed or tested to date.

In the current study we explore the spectrum of *MET* resistance mutations to type I and II MET inhibitors when administered as single agents or in combination with one another. We demonstrate that a combination of type I and II MET inhibitors is the most effective strategy at reducing the development of MET secondary mutations and should be explored in future clinical trials.

Materials and Methods

Antibodies and Compounds

Antibodies against phospho-MET (Tyr1234; sc-101736; RRID:AB_2143892) and HSP90 (sc-7947; RRID:AB_2121235) were purchased from Santa Cruz Biotechnology; total-MET (D1C2; #8198; RRID:AB_10858224) and anti-rabbit IgG-HRP (#7074; RRID: AB_2099233) from Cell Signaling Technology; Savolitinib, crizotinib, cabozantinib, and glesatinib were purchased from Selleckchem; merestinib from MedChem Express and Selleckchem. Chemical structures of the inhibitors are provided in Supplementary Fig. S1.

Expression vectors

Human TPR-MET cDNA was amplified from the pBabe-puro TPR-MET vector - a gift from Bob Weinberg's lab (Addgene; RRID:Addgene_10902) and subcloned into pDNR-dual (BD Biosciences) via the *XhoI* and *HindIII* restriction sites as described previously (27). The TPR-MET secondary mutations were introduced using the QuikChange Lightning Site-Directed Mutagenesis Kit (Agilent Technologies) and mutagenic primers listed in Supplementary Table S2. All constructs were confirmed by DNA sequencing. Constructs

were shuttled into the retroviral expression vector JP1540 using the BD Creator™ System (BD Biosciences).

Cell lines

HEK-293T cells were purchased from ATCC (in 2009) (RRID:CVCL_0063), cultured in DMEM, supplemented with 10% FBS, streptomycin and penicillin and authenticated using the Promega GenePrint 10 System at the RTSF Genomics Core at Michigan State University in August 2016. Ba/F3 cells were a generous gift from the lab of Dr. David Weinstock (2014) (RRID:CVCL_0161). Transformed Ba/F3 cells were maintained in RPMI1640 supplemented with 10% FBS, streptomycin and penicillin. NIH-3T3 were purchased for this study from ATCC (RRID:CVCL_0594) and maintained in DMEM supplemented with 10% FCS, streptomycin and penicillin. All cell lines used in the study tested negative for mycoplasma as determined by the Mycoplasma Plus PCR Primer Set (Agilent) throughout the study.

Generation of drug resistant cells

Ba/F3 cells expressing WT TPR-MET were exposed to 50 μg/mL of ENU (Sigma Aldrich) for 24 hours, washed and expanded in complete growth media. Recovered expanded cells were then seeded at 3,000 cells/well in 96-well plates (5 plates per drug treatment) in the presence of MET TKIs at concentrations and combinations described earlier. Drug-containing culture medium was refreshed and resistant clone emergence monitored once weekly. Individual drug resistant clones were isolated, expanded and subjected to DNA extraction. The TKD of resistant clones was PCR-amplified and Sanger-sequenced using primers listed in Supplementary Table S2. For Fig. 1, ddPCR was also performed on DNA extracts using primers and probes listed in Supplementary Table S2.

Viral transductions

HEK-293T cells were transfected with the retroviral construct in combination with the pAmpho to provide the envelope (Takara) using FuGENE® HD Transfection Reagent (Promega) per manufacturer's protocol. Viral supernatants were harvested 48 hours post-transfection, filtered, added to preplated cells along with 10 μg/mL or 15 μg/mL polybrene, for NIH3T3 and Ba/F3 cells, respectively, and centrifuged for 1 hour at 2100 rpm. Cells with successful retroviral integration were selected with 1-2 μg/mL puromycin. For *in vivo* studies, TPR-MET mutant Ba/F3 cell lines (Y1230H; G1163R; L1195V; F1200I) were luciferized with commercially produced CMV-Firefly luciferase lentivirus using the protocol provided by the manufacturer (Cellomics Technology; Cat. # PLV-10128). Resulting luciferized cell lines were functionally validated and MAP tested prior to implantation.

Drug treatments and Western blotting

NIH3T3 stably expressing each TPR-MET WT or mutant construct were seeded in 6-well plates at 600,000 cells/well and treated with the indicated TKIs and concentrations for 4 hours. At the end of treatment, cells were washed and lysed with RIPA lysis buffer containing protease and phosphatase inhibitors. Western blotting, and immunoblotting were done as described previously (12). Blots were developed on Amersham Imager 600 (GE

Healthcare Life Sciences). Phospho- and total MET signal was assessed at ~65kDa (the apparent size of TPR-MET).

MTS growth and viability assay

WT TPR-MET or mutant TPR-MET-dependent (IL-3 independent) Ba/F3 cells were seeded at 4,000 cells/well of 96-well round bottom plates and treated with dose-escalated MET TKIs as shown in Fig. 1F for 72 hours. Growth and viability were assessed by MTS assay according to previously established methods (12). Experimental points were set up in 6 to 12 technical replicates and average IC50 values were calculated based on at least 3 biological replicates.

Incucyte growth assay

Individual TPR-MET mutant Ba/F3 cell lines were seeded in 96-well round bottom wells at 30,000 cells/well and allowed to pool into the center of the well for 6 hours before imaging. Growth rate of individual TPR-MET mutant Ba/F3 cell lines was monitored and analyzed using Incucyte ZOOM (Essen BioScience) and the 2016b software as outlined previously (12).

MET specific droplet digital PCR assay

Taqman dye-labeled probes which specifically bind to *MET* D1228N, *MET* G1163R, L1195V, F1200I and Y1230H and correspondent primers for ddPCR assays were custom designed and ordered from ThermoFisher and IDT, respectively. Sequences of primers and probes are listed in Supplementary Table S2. ddPCR reagents were manufactured by Bio-Rad. ddPCR reactions were cycled in a thermocycler (BioRad) under the following cycling conditions: 95 °C × 10 min (1 cycle), 40 cycles of 94 °C × 30 s and 57 °C × 1 min, and 10 °C hold. PCR product fluorescence was evaluated on a Bio-Rad QX200 ddPCR reader as previously described. All samples were run in triplicates. Signals were quantified using the QuantaSoft (ver 1.6.6) software that accompanied the QX200 reader. Poisson concentrations were calculated by QuantaSoft, and mutant *MET* allele frequencies were determined.

In vitro combination effect and synergy studies

To determine synergy between two MET TKIs, four secondary mutant TPR-MET Ba/F3 cell lines containing the following mutations – Y1230H; G1163R; l1195V; F1200I - were admixed at a density of 175 cells/mutant/well (700 cells/well), seeded in a white 384-well plate format and treated with 6-10 different concentrations of each drug (n=6 replicates/drug combination). Single mutant TPR-MET Ba/F3 cells seeded at 700 cells/well were used to determine the absence of drug interactions on the molecular level. Endpoint analyses were performed after 72 hours of treatment using CellTiter Glo® (Promega Cat#G7570, USA). Bliss independence and synergy/antagonism calculations were performed and visualized by Combenefit (28).

Molecular docking studies

Co-crystal structures of MET kinase domain in complex with PF-04217903 (capmatinib analog) or merestinib (type II kinase inhibitor) were retrieved from Protein Data Bank (PDB

code 3ZXZ and 4EEV) and processed using Protein Preparation Wizard (Schrödinger LLC, New York, 2018). Protein-ligand structures were processed using the Protein Preparation Wizard (Schrödinger LLC, New York, 2018) as follows: addition of all hydrogens, assignment of bond orders, deletion of all water molecules, capping termini. Any missing side chains and missing loops were filled by using prime module (Schrödinger Release 2018-4: Prime, version 5.4) integrated within Protein Preparation Wizard. All residues of the proteins were then parameterized using OPLS2005 force field (29). Restrained minimization was performed until the converged average root mean square deviation (RMSD) of 0.3 Å was reached for heavy atoms. The MET mutant (F1200I) was generated by simple amino acid substitution and the geometry was optimized using of OPLS2005 force field. Docking studies of capmatinib and merestinib on MET kinase domain (WT and F1200I mutant) were carried out using GLIDE module (Small-Molecule Drug Discovery Suite 2018-4: Glide, version 8.1) in the Schrödinger package. A docking grid defining MET kinase domain was generated mainly considering the binding pocket of the MET inhibitors. Ligands (capmatinib and merestinib) were prepared using the Macromodel module (Schrödinger Release 2018-4; version 12.2) of the Schrödinger packages.

Molecular dynamics simulations

Molecular dynamics (MD) simulations of the complexes of MET kinase domain (WT and F1200I mutant) with these inhibitors (merestinib and capmatinib) were performed using the Desmond (Desmond Molecular Dynamics System, version 5.6; Maestro-Desmond Interoperability Tools, version 5.6,) in the Schrödinger 2018-4 software. Predefined TIP3P water model was utilized to simulate water molecules using OPLS2005 force field. Orthorhombic periodic boundary conditions were set up to specify the shape and size of the repeating unit buffered at 10 Å distances. In order to neutralize the system electrically, sodium ions were randomly placed in the solvated system to balance the system charge. After building the solvated system containing the protein in complex with the ligand, the system was minimized and relaxed using default protocol integrated within Desmond module using OPLS2005 force field parameters. Molecular dynamics simulations were carried out with the periodic boundary conditions in the NPT (isothermal and isobaric simulations) ensemble. Nose–Hoover thermostat algorithm (30) and Martina-Tobias-Klein method (31) were adopted for constant-temperature (300 K) and isotropic pressure (1 atm), respectively. The calculations were carried out by running the 100 ns NPT production simulation and saving the configurations. Trajectory was obtained at 100 ps intervals.

In vivo efficacy studies

All *in vivo* mouse studies were performed at the Dana-Farber Cancer Institute, Boston, USA in accordance with the guidelines approved by the Institutional Animal Care and Use Committee (IACUC) of Dana-Farber Cancer Institute. Female SHO (SCID Hairless Outbred) mice were purchased from Charles River Laboratories (Wilmington, MA, USA) for the tumor growth and efficacy studies. Initially, we tested the growth of TPR-MET mutant cell lines (F1200I, Y1230H, G1163R and L1195V) by injecting 2 x 10^6 cells in 100 μL PBS subcutaneously in the right flank of individual mice. For efficacy study, 0.5 x 10^6 million cells per each TPR-MET mutant cell lines were admixed *ex vivo* in a total 100 μL PBS and injected subcutaneously. Twenty-four hours after implantation,

mice were randomized to 10 mice/treatment arm and treated for 18 days by oral gavage as follows: Vehicle (10% gum Arabic, once daily + 0.5% methyl cellulose, twice daily); capmatinib, 30 mg/kg twice daily (vehicle: 0.5% methyl cellulose); merestinib, 24 mg/kg once daily (vehicle: 10% gum Arabic); and the combination of capmatinib and merestinib. For both studies, tumor size and body weight (BW) were monitored twice weekly, and mice were euthanized once the average tumor volume (TV) exceeded 2000 mm^3 or if the tumors became necrotic TV was calculated as follows: TV (mm^3)=length×width×width×0.5. BLI images of luciferized tumors were acquired once a week as follows: The mice were anesthetized using isoflurane and injected interperitoneally with 200μL of D-luciferin substrate (PerkinElmer 122799; 15mg/ml; 150mg/kg). Images were generated using the IVIS Lumina imaging system (PerkinElmer) 15 minutes post-injection. The images generated were analyzed in the Living Image software (PerkinElmer). At the end of treatment, mice were euthanized and tumors excised and flash frozen in liquid nitrogen and stored at −80°C until analysis by ddPCR. One-way ANOVA, assuming normal distribution and equal variance, and Holm-Sidak multiple comparison test was used to compare efficacy of each single agent to their combination. TV from day-18 was compared for estimation of synergy using Bliss definition of drugs' independence as described under "Treatment interaction in the presence of control group" section of a previously published method (32) (Supplementary Materials and Methods). $P \leq 0.05$ was considered significant.

TPR-MET analysis of tumor content

The presence and % contribution of each mutant TPR-MET Ba/F3 cell line to the tumors harvested on day 18 of treatment was determined by ddPCR performed on the total tumor gDNA. For comparison purposes, the % contribution of each mutant cell line was further expressed in terms of the relative tumor volume they comprised (Fig. 5C), assuming no differences in size between the mutant Ba/F3 cells or overall tumor composition. Genomic DNA from tumor samples was further subjected to a NGS using Resolution Bio ctDx assay. After sequencing, unique reads were generated and aligned to human reference genome hg19. The mouse contribution to reads was calculated using mouse-specific SNVs. Allele frequencies of DNA originating from human were reported at specified loci.

The data generated in this study are available within the article and its supplementary data files.

Results

Type I and type II MET TKIs differ in their propensity to induce resistant outgrowth

With the emergence of studies reporting on secondary MET mutations resistant primarily to the more established type I inhibitors, we sought to compare a panel of type I TKIs (type Ia: crizotinib; type Ib: savolitinib, capmatinib) and type II TKIs (cabozantinib, glesatinib, merestinib) for their ability to delay the emergence of resistance and/or to minimize the number of emergent resistant clones. Simultaneously, we aimed to characterize each TKI with regards to its efficacy against MET secondary mutations. We generated a MET-dependent Ba/F3 cell model by transforming IL3-dependent parental Ba/F3 cells with the oncogenic fusion TPR-MET. TPR-MET is the product of a chromosomal rearrangement,

fusing a protein dimerization domain (TPR) to the MET TKD, which eliminates the regulatory extracellular and juxtamembrane domains, including the tyrosine-binding site for the E3 ligase c-Cbl (Y1003). As such, TPR-MET is rendered constitutively activate and strongly oncogenic (2,33). The fusion between the two protein partners occurs just upstream of Asp1010 of MET and therefore contains the entire MET TKD. We performed an ENU mutagenesis assay, an experimental approach that has previously led to the discovery of clinically relevant drug resistance mutations to EGFR TKIs and HER2 TKIs (34-36). ENU-exposed TPR-MET Ba/F3 cells were subjected to long-term treatment with 100 nM or 500 nM of each MET TKI as monotherapy and the emergence of resistant clones was monitored weekly (Fig. 1A). The glesatinib treatment arm was eventually eliminated from this analysis, due to the drug's inability to inhibit growth in any wells at any tested concentration regardless of the MET TKD mutational status, possibly due to the drug's *in vitro* instability. Of the 300 seeded wells per TKI, crizotinib exhibited the highest number of outgrowing resistant clones at 100 nM, with 70% of all wells containing a resistant clone. This was followed by savolitinib and cabozantinib, with 17% and 13% of seeded wells showing resistant outgrowth, respectively. At the lower concentration, capmatinib and merestinib exhibited superior activity for the above metric with 3% and 6% resistant clones, respectively. At the higher concentration, all tested TKIs effectively prevented the emergence of resistance with ≤1% outgrowing wells.

For all drug treatment arms, at least 50% of the emerged resistant clones were collected for DNA extraction, PCR amplification of the MET TKD and subsequent Sanger sequencing of the TKD to identify putative acquired resistance-imparting secondary mutations (Fig. 1B). Vast majority of the resistant clones collected from the drug treatment arms at either concentration contained a secondary mutation in the MET TKD, with the exception of the 100 nM cabozantinib treatment arm, in which only 35% of the sequenced resistant clones harbored a secondary MET kinase mutation, with the remaining clones displaying acquired resistance of unknown, MET kinase independent, etiology. This discordance disappeared in the 500 nM cabozantinib treatment arm with 100% of the sequenced clones presenting with a putative resistance-driving mutation in the MET TKD. Thirty of the 300 emerged clones in the 500 nM glesatinib arm were chosen at random and sequenced, but presumably due to those clones not being truly structurally drug resistant, only 2 of them carried a secondary mutation in the MET TKD (Fig. 1B).

Treatment with single agent type I or type II MET TKIs gives rise to distinct sets of secondary mutants.

Sanger sequencing of the MET TKD amplified from the DNA of TPR MET Ba/F3 cell clones resistant to single agent MET TKIs revealed trends in both molecular location and identity of the acquired mutations emerging post-treatment. The V1155L mutation, in a residue located in the N lobe of MET TKD upstream of the hinge region, was identified as the most frequent mutation emerging post crizotinib treatment (94.5%) (Figs. 1C-E). Two of those had a concomitant Y1230N or Y1230H mutation. V1155L mutation was shared with only savolitinib, a type Ib inhibitor, however, its share of the total secondary mutation count was significantly lower (3%). Mutations at the Y1230 residue, one of the tyrosines within the activation loop of MET, were common to all 3 type I TKIs, type Ia crizotinib and type

Ib savolitinib and capmatinib, and was most frequently seen with savolitinib and capmatinib, at 94% and 75%, respectively. We documented substitutions of Y1230 for all Asp, His, Asn or Cys, however, there was no correlation between the aa substitution distribution and the treatment arm. Our group has previously reported on the mechanistic underpinnings of resistance to savolitinib rendered by the MET D1228V mutation (18). In our single agent ENU screen, substitutions of the D1228 residue with Tyr, Asn, or Gly were associated with type Ib inhibitors savolitinib and capmatinib treatment, with 6% and 16% incidence, respectively (Figs. 1C-E). As expected, the presence of the G1163R solvent front mutation among the crizotinib resistant mutants reflects the difference in the structural requirement for binding between type Ia and Ib inhibitors, representing a vulnerability for crizotinib but not savolitinib or capmatinib. A single case of a mixed M1211L/V mutation, a C-lobe aa residue immediately upstream of the activation loop, emerged following treatment with capmatinib, suggesting the involvement of this residue in capmatinib binding. Cabozantinib, a type II MET TKI, gave rise to a broader array of unique mutants than any other TKI in the panel, with C-lobe mutations in F1200 (F1200V/L/I) at 43.8%, and the hinge Y1159N mutation at 25% being the most represented. Cabozantinib further gave rise to G1163E, a solvent front residue shared with type Ia crizotinib, L1195F in the αE helix just upstream of F1200, and one case each of 2 unique mutations S1236R and H1238R, both located within the activation loop. Finally, mutations in F1200 in the β6 strand of MET were shared by and exclusive to the three tested type II TKIs. All the merestinib resistant clones had a F1200 mutation (F1200V/I/L), one case of which had a concurrent L1195F mutation, and even though our glesatinib data are complex to interpret, the only identified secondary mutation in the 30 sequenced glesatinib resistant clones was F1200L in 2 clones.

Next, we selected representative mutations identified in the ENU screen and constructed them in the original WT TPR-MET expression vector. We then transformed Ba/F3 cells with these constructs and established stable Ba/F3 cell lines driven by TPR-MET carrying one of the secondary mutations. The inhibitory activity of each type I or type II MET TKI was assessed against all mutants, using 72-hour dose-escalated MTS growth and viability assay. The IC50 values of each mutant cell line was determined for all drugs (Fig. 1F). We show D1228 and Y1230 mutations to be moderately resistant to crizotinib and strongly resistant to both savolitinib and capmatinib, while retaining sensitivity to all type II TKIs, although not to the extent of WT TPR-MET. G1163R and L1195V represent a unique set with mutations of concordant sensitivity and resistance profile for both type I and type II MET TKIs. These two mutations are slightly to moderately resistant to crizotinib, cabozantinib and glesatinib, but strongly sensitive to savolitinib and capmatinib. The Y1159N and M1211L mutations exhibit similar trends, however, their resistance-imparting capacity against crizotinib and cabozantinib is diminished compared to G1163R and L1195V, and against glesatinib not considerably different from the WT. The M1211L mutation was only weakly resistant overall. As expected, the most commonly identified crizotinib resistant mutation, V1155L, exhibited moderate resistance to crizotinib and mild resistance to savolitinib and capmatinib, but was sensitive to all type II inhibitors. Finally, F1200I was strongly resistant to cabozantinib and glesatinib, moderately to merestinib and crizotinib, and mildly to savolitinib and capmatinib. Merestinib had the broadest, while crizotinib most

narrow activity against the tested mutants as evidenced by the therapeutic index comparison (Fig. 1G).

Combination of type I and type II MET TKIs prevents emergence of resistance *in vitro*

Given that the emergence of resistance following treatment with any single agent MET TKI appears inevitable, albeit at different rates and with different secondary mutations, we sought to determine the efficacy of various combinations of type I and type II MET TKIs in preventing or minimizing resistance emergence *in vitro*. We employed a similar experimental approach as with single agents described earlier - TPR-MET Ba/F3 cells were subjected to ENU mutagenesis, followed by a long-term treatment with 300 nM of each MET TKI as monotherapy or in combinations and the emergent resistant clones were counted and harvested weekly (Fig. 2A, B). In line with our earlier single agent data, crizotinib and cabozantinib monotherapies were the least effective at preventing resistant outgrowth, with 35.7% and 53.3% of all wells (n=300 per drug), respectively, containing a drug resistant clone. At this concentration, capmatinib, savolitinib, and merestinib were highly effective at suppressing the emergence of resistance, with only 0.3%, 3.0%, and 1.3% of seeded wells exhibiting outgrowth, respectively. Given the cross-resistance profiles and relative potency (Fig. 1E-G), it is not surprising that the combination of crizotinib and cabozantinib in particular failed to thwart the emergence of resistance. The combination resulted in 24.3% of the treated wells containing a resistant clone, only 32% and 54% fewer than with crizotinib or cabozantinib monotherapy, respectively (Fig. 2A). In contrast, the combinations of type I and type II inhibitors with smaller cross-resistance proved significantly more compelling – the crizotinib/merestinib, savolitinib/cabozantinib, and savolitinib/merestinib combinations all potently reduced the incidence of resistant outgrowth, with only 0.3%, 1% and 1.3%, respectively, of seeded wells escaping inhibition (n=300 per treatment). Strikingly, capmatinib combinations yielded no resistant clones. In addition, we noted differences in the latency of resistance emergence between the individual treatment arms (Fig. 2B). While single agents crizotinib, savolitinib, and cabozantinib, and the crizotinib/cabozantinib combination showed evidence of resistance emergence within the first week of treatment, and merestinib and capmatinib within the first 2 weeks of treatment, the crizotinib/merestinib and savolitinib/merestinib combinations started giving rise to resistant clones only at week 3, and savolitinib/cabozantinib at week 5.

To better quantify individual mutant MET clones in a mixture of cells, we developed a digital droplet PCR (ddPCR) assay for a number of prevalent secondary mutations. For this purpose, genomic DNA was extracted from a representative number of resistant clones and probed for the presence of mutations identified in the original single agent screen using ddPCR. Orthogonally, traditional Sanger sequencing was performed on the MET TKD PCR-amplified from the same genomic DNA extracts. Sequencing was performed in order to assess the identity, frequency and distribution of MET TKD secondary mutations, as well as distinguish cases with MET TKD independent resistance. Both methods exhibited high specificity concordance in detecting a mutant residue (100%), and 95% sensitivity relative to each other (Supplementary Table S3). Some of our ddPCR probes demonstrated low cross-reactivity towards other mutations, detecting other non-WT aa substitutions in addition to those they were designed against – L1195V detected L1195F; Y1230H detected

Y1230C; F1200I detected F1200V and F1200L – however, there were no false mutant positive calls when referenced against our Sanger sequencing data (Supplementary Table S3). The combined sequencing data established that at 300 nM, the tested drug treatments were permissive of mutations at only 4 MET TKD aa residues – Y1230, G1163, L1195 and F1200 (Fig. 2C). Specifically, crizotinib monotherapy gave rise to 3 - G1163R at 92.3%, Y1230H/C at 5.2%, and F1200V at 2.6%. Following savolitinib or capmatinib monotherapy, 100% of the sequenced resistant clones were positive for Y1230H/C. Cabozantinib monotherapy yielded resistant clones consisting of 85.1% G1163R, 8.5% L1195F, 4.3% F1200V and a single case of a dual mutant G1163R/L1195F. Merestinib, like at other tested concentrations, gave rise to a mutant at F1200 - 100% resistant clones carried F1200V. The crizotinib/cabozantinib treatment arm gave rise to the G1163R (97.3%) and F1200V (2.7%) mutants, neither of which is adequately targeted by either drug alone based on our prior data (Fig. 1E-G). This is also in line with the high incidence and short latency of resistant outgrowth seen with this combination earlier. Notably, none of the clones emerging in the remaining three combination treatment arms (crizotinib/merestinib, savolitinib/merestinib, savolitinib/cabozantinib) contained a secondary MET TKD mutation, suggesting that the resistance mechanism was not MET TKD specific. In the remaining treatment arms, all resistant clones were positive for a secondary mutation in the MET TKD. Finally, to biochemically confirm MET TKI engagement, or lack therefore, of WT or mutant MET, we transformed NIH-3T3 cells with the WT or mutant TPR-MET expression vectors and subjected them to a 3h MET TKI treatment (Fig. 2D). A Western blot signaling analysis of phospho-MET levels was performed to evaluate the impact of the mutations on the ability of each drug to inhibit MET phosphorylation. This study largely corroborated our growth inhibition profiling data (Fig. 1F) - we observed a dose-dependent reduction in TPR-MET phosphorylation in WT TPR-MET cells treated with all six inhibitors. The Y1230H mutation prevented phosho-MET inhibition by all type I inhibitors, but especially both type Ib capmatinib and savolitinib. In contrast, this mutation had no effect on sensitivity to any type II TKIs. The solvent front G1163R mutation diminished the inhibitory effects of crizotinib and cabozantinib, while L1195V negatively affected the activity of crizotinib and all type II inhibitors, but remained strongly sensitive to both type Ib TKIs. Finally, the F1200I mutations, especially, appeared never fully inhibited by any of the MET TKIs, regardless of the type, even though type Ib inhibitors performed markedly better than crizotinib or type II TKIs (Fig. 1F and 2D). Collectively, we hypothesize that merestinib combined with a type Ib inhibitor would be an optimal MET TKI combination to prevent, delay, and/or diminish the extent of resistant outgrowth.

Combination of capmatinib and merestinib achieve cellular synergy and highest combined dose response *in vitro*

To evaluate MET TKI type I/type II combination effect, we employed the Bliss independence dose-response surface model. We admixed four TPR-MET Ba/F3 cell lines, each containing a secondary mutant identified in our ENU study (Fig. 2) – Y1230H; G1163R; L1195V; F1200I, at equal ratios and performed *in vitro* drug combination studies, assaying for cell viability. For all tested combinations, synergy was observed on the cellular level when the mixture of the 4 secondary MET mutants was treated (Fig. 3A), but not on the molecular level when a single mutant was treated with these combinations (Fig. 3B),

given that only one TKI can bind at any given time to a single MET molecule, but two TKIs can act simultaneously and to varying degrees on a mixture of mutant cell lines. Synergies shown in Fig. 3A highlight the potential of these combinations to target multiple pre-existing secondary MET mutant clones expected to exist in mutant MET tumors. The capmatinib/merestinib combination achieved the best combined dose response of the combinations tested (Fig. 3C).

Structural insights into the requirement of MET F1200 for merestinib or capmatinib binding

Despite the apparent superiority of merestinib as a type II MET TKI, its vulnerability to MET F1200 mutations is a liability. Based on 1) the ability of capmatinib to most prominently minimize resistance emergence (Fig. 1D, 2A-C), 2) its resistance profile diverging from that of merestinib (Fig. 1E-G), and 3) relatively high activity against the particularly refractory F1200X mutations, we carried out 100ns molecular dynamic (MD) simulations to model the interaction of capmatinib or merestinib with either WT or MET F1200I mutant and assessed the drugs' reliance on the WT F1200 aa residue for optimal binding (Fig. 4A-D). An aromatic cluster in which aromatic residues of Phe and Trp are in close proximity to each other to make aromatic-aromatic interactions are often observed in protein structures. Building upon the published crystal structure of merestinib-bound MET, we first show that three phenyl rings from the F1134/F1200/fluorophenyl tail of merestinib form an aromatic cluster, which amplifies the binding affinity of merestinib for MET (Fig. 4A). However, in the presence of a mutation in F1200, in this case F1200I, this stabilizing aromatic cluster is fully disrupted, resulting in a weaker overall binding affinity of merestinib for MET (Fig. 4B). Capmatinib has a very different mode of binding, one that depends on the interaction with the activation loop of MET, which is a representative binding pattern for a MET type I inhibitor. In MET with WT activation loop, capmatinib makes an effective π-π stacking interaction with Y1230 (Fig. 4C) and depends for its full activity on the integrity of this aa residue. In contrast, our simulations demonstrate that the F1200 aa residue has no bearing on the interaction of capmatinib with MET (Fig. 4C,D). We show that in both WT and F1200I mutant MET, F1200I mutation has no influence on the π-π stacking and is therefore not expected to affect the affinity of capmatinib for MET (Fig. 4D). Collectively, our MD simulation studies provide more confidence in our selection of merestinib and capmatinib for a MET TKI combination treatment, with the intent to provide the broadest possible coverage of anticipated acquired secondary MET mutations, as a strategy to prevent or delay the emergence of resistance.

The combination of capmatinib and merestinib diminishes the emergence of resistance *in vivo*.

Next, we assessed the efficacy of the capmatinib/merestinib combination *in vivo*. *In vivo* efficacy studies are largely complicated by the unavailability of both naïve and drug resistant patient-derived *MET*ex14 mutant cell lines. To circumvent this, we developed an *in vivo* mouse xenograft assay, using admixed TPR-MET Ba/F3 cells carrying different MET secondary mutations. First, TPR-MET mutant Ba/F3 cells containing one of the following mutations – G1163R; Y1230H; L1195V; F1200I – were compared for growth rates. The growth rate of the G1163R; L1195V; F1200I mutants didn't differ significantly, however that of Y1230H exhibited a slower growth rate *in vitro* (Supplementary Fig.

S2A). Cognizant of the possibility that growth rate may be further confounded *in vivo*, we injected each mutant subcutaneously, and compared relative tumor growth over the span of 3 weeks (Supplementary Fig. S2B). Under these conditions, we found the Y1230H; L1195V; F1200I mutants to have comparable growth rates, however, G1163R proliferated faster. Ba/F3 cell models have a propensity to metastasize *in vivo*. Therefore, we luciferized all 4 TPR-MET Ba/F3 cell lines for bioluminescence monitoring and weighed the organs that are known to be common metastatic sites at the end of the study to estimate the metastatic potential of each cell line. The spleen, lung and liver in the TPR-MET F1200I and L1195V groups were slightly enlarged compared to those of TPR-MET G1163R and Y1230H (Supplementary Fig. S2C), however, bioluminescence imaging (BLI) did not detect metastases in the abdomen, thorax or lymph nodes (Supplementary Fig. S2D). Hence, we concluded that luciferase-based assessment of metastatic growth in addition to measurement of the primary tumor site was not warranted.

To compare the efficacy of single agent merestinib, capmatinib and the combination, we admixed the four TPR-MET mutant Ba/F3 cell lines at equal ratios *ex-vivo* and implanted them subcutaneously. 24 hours post-implantation, vehicle or MET TKI treatment was administered for a total of 14 days. While neither single agent treatment arm resulted in tumor growth inhibition compared to the vehicle, the combination treatment significantly reduced tumor growth – by average of 50.4% relative to capmatinib and 43.3% relative to merestinib alone (Fig. 5A, Supplementary Fig. S2E, F). Notably, the combination was well tolerated at the TKI doses used (Fig. 5B), as illustrated by no loss in average body weight, a standard surrogate for drug-induced toxicity in murine drug efficacy studies. Next, we used ddPCR to quantify the individual contribution of each TPR-MET mutant to the final tumor outgrowth and expressed each as a percentage of the final tumor volume (Fig. 5C). Despite considerable variations in tumor volume within each treatment arm, relative mutant distribution remained consistent between tumor samples irrespective of the tumor volume. As expected, merestinib monotherapy successfully barred the growth of the Y1230H mutant, while the capmatinib monotherapy arm was especially effective in eliminating the G1163R mutant. In both single agent treatments, this came at the cost of enabling the outgrowth of the more resistant mutants - G1163R for merestinib and Y1230H for capmatinib. While both mutants virtually disappeared in the combination arm treatment, neither drug, alone or in combination, was effective against the F1200I mutant. No conclusions could be drawn about the efficacy against the L1195V mutant in this study, due to its inadvertent elimination from the vehicle arm tumors. This phenomenon was also observed *in vitro* (Supplementary Fig. S3A), hinting at the possibility that the L1195V mutant has an intrinsic growth disadvantage when mixed with the other TPR-MET mutants. We therefore repeated the *in vivo* efficacy study only with the L1195V mutant cells and demonstrated that capmatinib alone effectively inhibited tumor growth, while merestinib was ineffective and didn't further improve efficacy when combined with capmatinib (Supplementary Fig. S3B). As with the original *in vivo* efficacy study, the positive trend in body weight for all treatment arms indicates that all treatments are well tolerated in this murine model (Supplementary Fig. S3C). Collectively, while the combination permitted the outgrowth of the F1200I mutant, and hence, wasn't curative, it had a significant inhibitory activity in tumors, as compared to the single agents. The day 18 ratio of surviving fraction (SF) under Bliss independence to SF of

the combination group yielded a statistically significant 46% synergy (one-sided p = 0.038), (Table 1).

Discussion

With NGS bringing to the forefront *MET*ex14 alterations as a relatively common driver in cancers, including NSCLC (8,37), several effective MET TKIs have been developed responding to the previously unmet need of this cancer subtype (38). Unfortunately, as with most other TKI therapies used as single agents, the acquisition of secondary kinase domain resistant mutations and/or activation of bypass signaling dictate that any one TKI treatment is rarely curative. Thus, uncovering the biology behind MET TKI resistance in lung cancer and devising strategies to overcome it has been front and center in lung cancer research in recent years.

In this study, we characterized MET TKIs with respect to the nature of the secondary mutants they produced and provided a rationale for a specific MET TKI combination that could prevent, delay or diminish resistance *in vivo* and could eventually extend treatment benefits in patients. Our data were consistent with two related preclinical studies published earlier (26,39). The efficacy of resistance suppression was inversely correlated with drug concentration. At lower concentrations, the variety of total secondary mutations emerging in response to treatment to type I or II inhibitors was greater – 10 mutated aa residues; 17 distinct aa substitutions. At higher concentrations, both the diversity and the number of resistant clones decreased as predicted, selecting for secondary mutations imparting higher degree of resistance. The heterogeneity of mutations we observed was smaller than that previously reported by e.g. Fujino et. al (26), however, differences in drug concentrations and in the target itself (TPR-MET vs. METex14 mutant) may explain this discrepancy. Pertinently, our study identified several mutations observed in clinical settings - Recondo et. al (16) have identified MET TKI resistant patients with on-target single and polyclonal mutations in a number of aa residues, including G1163, L1195, D1228, Y1230. While most of these mutations were acquired while on crizotinib treatment, there was a case of glesatinib resistant patient who carried the L1195V mutation, further corroborating our data. Since type II MET TKIs, other than cabozantinib, remain in various stages of clinical development, patients resistant to type II TKIs are represented at significantly lower numbers than those resistant to e.g. crizotinib, which could account for the absence of F1200 mutations observed in resistant lung cancer patients to date. MET F1200I and F1200V mutations have been found in papillary renal cell carcinoma, however, their impact on MET TKI sensitivity was not established in this malignancy (40). Meanwhile, additional reports implicating D1228 and Y1230 mutations in type I MET TKI resistance in lung and other malignancies continue to grow in number (18,41-43)

Based on our *in vitro* studies and prior reports, the result of our *in vivo* studies indicating the sustenance of the F1200I Ba/F3 cell population in the combination treatment arm was surprising. Primarily, F1200X mutations are expected to impart resistance to type II inhibitors, by impacting the shape of the hydrophobic binding pocket in MET (44). Type I inhibitors may exhibit diminished affinity for F1200X mutant MET, possibly due to these mutations warping the substrate-binding pocket, resulting in an increased affinity for ATP.

However, neither our *in vitro* cellular assays, nor our MD simulation studies predicted this degree of ineffectiveness of capmatinib against MET F1200I. One possible explanation may lie in the experimental set-up, in which 100% of the injected TPR-MET Ba/F3 cells, by design, contained a secondary mutation at the time of implantation. However, the secondary mutant population dynamics, especially when in a mixture with WT or other mutants, is far from straightforward or predictable. In fact, mathematical models have shown that the initial fraction of resistant cells, and degree of selective pressure can profoundly affect drug response (45). It is therefore possible that with an IC50 of 29nM and IC90 of 56nM against the F1200I mutant (Fig. 1F), the dose and/or treatment schedule of capmatinib don't reach the threshold necessary to sufficiently inhibit the quickly proliferating F1200I mutant, given the high number of cells implanted. Our *in vivo* data (Fig. 5C) also indicate that the growth advantage of some mutants in the vehicle treated tumors (G1163R and F1200I), presumably at the cost of others (Y1230H and L1195V), may impact drug response. Interestingly, despite the low fraction of Y1230H in the harvested vehicle-treated tumors, capmatinib monotherapy still fell short of controlling this population, as evidenced by its prominent outgrowth in the single agent capmatinib arm. In contrast, the similarly low fraction of L1195V in the vehicle-treated tumors didn't outgrow inhibition in any of the treatment arms, however, L1195V was shown resistant to merestinib monotherapy in a follow-up *in vivo* efficacy study.

The key objective of our study was to use our *in vitro* findings as a rationale to combine two MET TKI's *in vivo* and assess the activity of the combination against especially prevalent secondary mutations emerging from our assays, and potentially driving resistance in patients as well. Factoring in the different modes of MET TKI binding and recognizing secondary mutations as an important determinant of these interactions is not a new concept. In fact, switching from one MET TKI to another based on their mode of binding in order to address resistant mutations that diverge in their sensitivities between type I and II TKIs has already met with some success in the clinic (16,18). However, the sequential treatment approach is bound to provide a therapeutic benefit only until another MET secondary mutant clone emerges. In addition, the period in-between treatments may enable the primary malignancy to select for both MET-dependent and MET-independent alterations, which may potentially render the newly arisen tumor unresponsive even to a MET TKI hypothesized to be effective. This provides an argument for administering two non-cross-resistant MET TKIs concurrently, whereby the outgrowth of major predicted preexisting secondary mutant clones can be effectively targeted in first line. While to our knowledge there is no clinical evidence of long-term efficacy and tolerability of any such MET TKI combination, examples drawn from clinical trials testing TKI combinations against other receptor tyrosine kinases provide encouragement. Among those, the type I EGFR TKIs dacomitinib combined with osimertinib (NCT03810807), or the combination of gefitinib and osimertinib validated preclinically as effective (35) and now shown as tolerable in a clinical trial (NCT03122717) are hoped to set precedent to such combination approaches. On the other side of the drug combination argument sits the theory hypothesizing that the "maximal kill" approach may unnecessarily increase selective pressure on tumor cells, promoting resistance evolution instead (46). Whether chronic maintenance of stable disease or a broader, more aggressive

treatment approach in form of first-line combinations is the answer to longer PFS and/or overall survival (OS) in patients is yet to be demonstrated.

With many MET inhibitors, FDA-approved or in development, it will be a challenge to distill with clinical trials how and when to administer MET TKIs in sequence or in combination. Mathematical modeling of the MET TKI resistant population may be useful in establishing the TKI dosing, sequence or combination. Finally, while we have shed light on drug resistance imparted by single MET secondary mutations, we predict that same conclusions cannot be drawn about multiple mutations existing in *cis*. Additional MET TKI profiling of secondary mutants in *cis*, their joint influence on the structural properties of the TKD and ensuing changes to MET TKI sensitivity need to be pursued.

Supplementary Material

Refer to Web version on PubMed Central for supplementary material.

Acknowledgments

This work was supported by The American Cancer Society (CRP-17-111-01-CDD to P.A.J.), the National Cancer Institute (R01CA135257; R01CA222823; R35 CA220497to P.A.J.), the Mugar Family Fund (to P.A.J.), the Goldstein Family Fund (to P.A.J.), and the Expected Miracle Foundation (to Y.K.).

References

1. Cortot AB, Kherrouche Z, Descarpentries C, Wislez M, Baldacci S, Furlan A, et al. Exon 14 Deleted MET Receptor as a New Biomarker and Target in Cancers. Journal of the National Cancer Institute 2017;109(5) doi 10.1093/jnci/djw262.
2. Peschard P, Fournier TM, Lamorte L, Naujokas MA, Band H, Langdon WY, et al. Mutation of the c-Cbl TKB domain binding site on the Met receptor tyrosine kinase converts it into a transforming protein. Molecular cell 2001;8(5):995–1004 doi 10.1016/s1097-2765(01)00378-1. [PubMed: 11741535]
3. Peschard P, Ishiyama N, Lin T, Lipkowitz S, Park M. A conserved DpYR motif in the juxtamembrane domain of the Met receptor family forms an atypical c-Cbl/Cbl-b tyrosine kinase binding domain binding site required for suppression of oncogenic activation. The Journal of biological chemistry 2004;279(28):29565–71 doi 10.1074/jbc.M403954200. [PubMed: 15123609]
4. Gandino L, Longati P, Medico E, Prat M, Comoglio PM. Phosphorylation of serine 985 negatively regulates the hepatocyte growth factor receptor kinase. The Journal of biological chemistry 1994;269(3):1815–20. [PubMed: 8294430]
5. Hashigasako A, Machide M, Nakamura T, Matsumoto K, Nakamura T. Bi-directional regulation of Ser-985 phosphorylation of c-met via protein kinase C and protein phosphatase 2A involves c-Met activation and cellular responsiveness to hepatocyte growth factor. The Journal of biological chemistry 2004;279(25):26445–52 doi 10.1074/jbc.M314254200. [PubMed: 15075332]
6. Tulasne D, Deheuninck J, Lourenco FC, Lamballe F, Ji Z, Leroy C, et al. Proapoptotic function of the MET tyrosine kinase receptor through caspase cleavage. Molecular and cellular biology 2004;24(23):10328–39 doi 10.1128/MCB.24.23.10328-10339.2004. [PubMed: 15542841]
7. Baek CM, Jeon SH, Jang JJ, Lee BS, Lee JH. Transforming variant of Met receptor confers serum independence and anti-apoptotic property and could be involved in the mouse thymic lymphomagenesis. Experimental & molecular medicine 2004;36(4):283–91 doi 10.1038/emm.2004.39. [PubMed: 15365247]
8. Frampton GM, Ali SM, Rosenzweig M, Chmielecki J, Lu X, Bauer TM, et al. Activation of MET via diverse exon 14 splicing alterations occurs in multiple tumor types and confers clinical sensitivity to MET inhibitors. Cancer discovery 2015;5(8):850–9 doi 10.1158/2159-8290.CD-15-0285. [PubMed: 25971938]

9. Cancer Genome Atlas Research N. Comprehensive molecular profiling of lung adenocarcinoma. Nature 2014;511(7511):543–50 doi 10.1038/nature13385. [PubMed: 25079552]
10. Paik PK, Drilon A, Fan PD, Yu H, Rekhtman N, Ginsberg MS, et al. Response to MET inhibitors in patients with stage IV lung adenocarcinomas harboring MET mutations causing exon 14 skipping. Cancer discovery 2015;5(8):842–9 doi 10.1158/2159-8290.CD-14-1467. [PubMed: 25971939]
11. Awad MM, Oxnard GR, Jackman DM, Savukoski DO, Hall D, Shivdasani P, et al. MET Exon 14 Mutations in Non-Small-Cell Lung Cancer Are Associated With Advanced Age and Stage-Dependent MET Genomic Amplification and c-Met Overexpression. Journal of clinical oncology : official journal of the American Society of Clinical Oncology 2016;34(7):721–30 doi 10.1200/JCO.2015.63.4600. [PubMed: 26729443]
12. Bahcall M, Awad MM, Sholl LM, Wilson FH, Xu M, Wang S, et al. Amplification of Wild-type KRAS Imparts Resistance to Crizotinib in MET Exon 14 Mutant Non-Small Cell Lung Cancer. Clinical cancer research : an official journal of the American Association for Cancer Research 2018;24(23):5963–76 doi 10.1158/1078-0432.CCR-18-0876. [PubMed: 30072474]
13. Vojnic M, Kubota D, Kurzatkowski C, Offin M, Suzawa K, Benayed R, et al. Acquired BRAF Rearrangements Induce Secondary Resistance to EGFR therapy in EGFR-Mutated Lung Cancers. Journal of thoracic oncology : official publication of the International Association for the Study of Lung Cancer 2019;14(5):802–15 doi 10.1016/j.jtho.2018.12.038.
14. Jamme P, Fernandes M, Copin MC, Descarpentries C, Escande F, Morabito A, et al. Alterations in the PI3K pathway drive resistance to MET inhibitors in NSCLC harboring MET exon 14 skipping mutations. Journal of thoracic oncology : official publication of the International Association for the Study of Lung Cancer 2020 doi 10.1016/j.jtho.2020.01.027.
15. Rotow JK, Gui P, Wu W, Raymond VM, Lanman RB, Kaye FJ, et al. Co-occurring Alterations in the RAS-MAPK Pathway Limit Response to MET Inhibitor Treatment in MET Exon 14 Skipping Mutation-Positive Lung Cancer. Clinical cancer research : an official journal of the American Association for Cancer Research 2020;26(2):439–49 doi 10.1158/1078-0432.CCR-19-1667. [PubMed: 31548343]
16. Recondo G, Bahcall M, Spurr LF, Che J, Ricciuti B, Leonardi GC, et al. Molecular Mechanisms of Acquired Resistance to MET Tyrosine Kinase Inhibitors in Patients with MET Exon 14-Mutant NSCLC. Clinical cancer research : an official journal of the American Association for Cancer Research 2020 doi 10.1158/1078-0432.CCR-19-3608.
17. Heist RS, Sequist LV, Borger D, Gainor JF, Arellano RS, Le LP, et al. Acquired Resistance to Crizotinib in NSCLC with MET Exon 14 Skipping. Journal of thoracic oncology : official publication of the International Association for the Study of Lung Cancer 2016;11(8):1242–5 doi 10.1016/j.jtho.2016.06.013.
18. Bahcall M, Sim T, Paweletz CP, Patel JD, Alden RS, Kuang Y, et al. Acquired METD1228V Mutation and Resistance to MET Inhibition in Lung Cancer. Cancer discovery 2016;6(12):1334–41 doi 10.1158/2159-8290.CD-16-0686. [PubMed: 27694386]
19. Ou SI, Young L, Schrock AB, Johnson A, Klempner SJ, Zhu VW, et al. Emergence of Preexisting MET Y1230C Mutation as a Resistance Mechanism to Crizotinib in NSCLC with MET Exon 14 Skipping. Journal of thoracic oncology : official publication of the International Association for the Study of Lung Cancer 2017;12(1):137–40 doi 10.1016/j.jtho.2016.09.119.
20. Dong HJ, Li P, Wu CL, Zhou XY, Lu HJ, Zhou T. Response and acquired resistance to crizotinib in Chinese patients with lung adenocarcinomas harboring MET Exon 14 splicing alternations. Lung cancer 2016;102:118–21 doi 10.1016/j.lungcan.2016.11.006. [PubMed: 27987579]
21. Zhang J, Yang PL, Gray NS. Targeting cancer with small molecule kinase inhibitors. Nature reviews Cancer 2009;9(1):28–39 doi 10.1038/nrc2559. [PubMed: 19104514]
22. Gherardi E, Birchmeier W, Birchmeier C, Vande Woude G. Targeting MET in cancer: rationale and progress. Nature reviews Cancer 2012;12(2):89–103 doi 10.1038/nrc3205. [PubMed: 22270953]
23. Cui JJ. Targeting Receptor Tyrosine Kinase MET in Cancer: Small Molecule Inhibitors and Clinical Progress. Journal of Medicinal Chemistry 2014;57(11):4427–53 doi 10.1021/jm401427c. [PubMed: 24320965]

24. Pargellis C, Tong L, Churchill L, Cirillo PF, Gilmore T, Graham AG, et al. Inhibition of p38 MAP kinase by utilizing a novel allosteric binding site. Nature structural biology 2002;9(4):268–72 doi 10.1038/nsb770. [PubMed: 11896401]
25. Recondo G, Bahcall M, Spurr LF, Che J, Ricciuti B, Leonardi GC, et al. Molecular Mechanisms of Acquired Resistance to MET Tyrosine Kinase Inhibitors in Patients with MET Exon 14-Mutant NSCLC. Clinical cancer research : an official journal of the American Association for Cancer Research 2020;26(11):2615–25 doi 10.1158/1078-0432.CCR-19-3608. [PubMed: 32034073]
26. Fujino T, Kobayashi Y, Suda K, Koga T, Nishino M, Ohara S, et al. Sensitivity and Resistance of MET Exon 14 Mutations in Lung Cancer to Eight MET Tyrosine Kinase Inhibitors In Vitro. Journal of thoracic oncology : official publication of the International Association for the Study of Lung Cancer 2019;14(10):1753–65 doi 10.1016/j.jtho.2019.06.023.
27. Sasaki T, Okuda K, Zheng W, Butrynski J, Capelletti M, Wang L, et al. The neuroblastoma-associated F1174L ALK mutation causes resistance to an ALK kinase inhibitor in ALK-translocated cancers. Cancer research 2010;70(24):10038–43 doi 10.1158/0008-5472.CAN-10-2956. [PubMed: 21030459]
28. Di Veroli GY, Fornari C, Wang D, Mollard S, Bramhall JL, Richards FM, et al. Combenefit: an interactive platform for the analysis and visualization of drug combinations. Bioinformatics 2016;32(18):2866–8 doi 10.1093/bioinformatics/btw230. [PubMed: 27153664]
29. Jorgensen WL, Maxwell DS, Tirado-Rives J. Development and testing of the OPLS all-atom force field on conformational energetics and properties of organic liquids. J Am Chem Soc 1996(118):11225–36.
30. Nosé S, . A unified formulation of the constant temperature molecular dynamics methods. J Chem Phys 1984(81):511.
31. Martyna GJ, Tobias DJ, Klein ML. Constant pressure molecular dynamics algorithms. J Chem Phys 1994(101):4177–89.
32. Demidenko E, Miller TW. Statistical determination of synergy based on Bliss definition of drugs independence. PloS one 2019;14(11):e0224137 doi 10.1371/journal.pone.0224137. [PubMed: 31765385]
33. Park M, Dean M, Cooper CS, Schmidt M, O'Brien SJ, Blair DG, et al. Mechanism of met oncogene activation. Cell 1986;45(6):895–904 doi 10.1016/0092-8674(86)90564-7. [PubMed: 2423252]
34. Zhou W, Ercan D, Chen L, Yun CH, Li D, Capelletti M, et al. Novel mutant-selective EGFR kinase inhibitors against EGFR T790M. Nature 2009;462(7276):1070–4 doi 10.1038/nature08622. [PubMed: 20033049]
35. Ercan D, Choi HG, Yun CH, Capelletti M, Xie T, Eck MJ, et al. EGFR Mutations and Resistance to Irreversible Pyrimidine-Based EGFR Inhibitors. Clinical cancer research : an official journal of the American Association for Cancer Research 2015;21(17):3913–23 doi 10.1158/1078-0432.CCR-14-2789. [PubMed: 25948633]
36. Kosaka T, Tanizaki J, Paranal RM, Endoh H, Lydon C, Capelletti M, et al. Response Heterogeneity of EGFR and HER2 Exon 20 Insertions to Covalent EGFR and HER2 Inhibitors. Cancer research 2017;77(10):2712–21 doi 10.1158/0008-5472.CAN-16-3404. [PubMed: 28363995]
37. Kurppa KJ, Liu Y, To C, Zhang T, Fan M, Vajdi A, et al. Treatment-Induced Tumor Dormancy through YAP-Mediated Transcriptional Reprogramming of the Apoptotic Pathway. Cancer cell 2020;37(1):104–22 e12 doi 10.1016/j.ccell.2019.12.006. [PubMed: 31935369]
38. Salgia R, Sattler M, Scheele J, Stroh C, Felip E. The promise of selective MET inhibitors in non-small cell lung cancer with MET exon 14 skipping. Cancer treatment reviews 2020;87:102022 doi 10.1016/j.ctrv.2020.102022. [PubMed: 32334240]
39. Tiedt R, Degenkolbe E, Furet P, Appleton BA, Wagner S, Schoepfer J, et al. A drug resistance screen using a selective MET inhibitor reveals a spectrum of mutations that partially overlap with activating mutations found in cancer patients. Cancer research 2011;71(15):5255–64 doi 10.1158/0008-5472.CAN-10-4433. [PubMed: 21697284]
40. Tate JG, Bamford S, Jubb HC, Sondka Z, Beare DM, Bindal N, et al. COSMIC: the Catalogue Of Somatic Mutations In Cancer. Nucleic acids research 2019;47(D1):D941–D7 doi 10.1093/nar/gky1015. [PubMed: 30371878]

41. Frigault MM, Markovets A, Nuttall B, Kim KM, Park SH, Gangolli EA, et al. Mechanisms of Acquired Resistance to Savolitinib, a Selective MET Inhibitor in MET-Amplified Gastric Cancer. JCO precision oncology 2020;4 doi 10.1200/PO.19.00386.

42. Li A, Yang JJ, Zhang XC, Zhang Z, Su J, Gou LY, et al. Acquired MET Y1248H and D1246N Mutations Mediate Resistance to MET Inhibitors in Non-Small Cell Lung Cancer. Clinical cancer research : an official journal of the American Association for Cancer Research 2017;23(16):4929–37 doi 10.1158/1078-0432.CCR-16-3273. [PubMed: 28396313]

43. Piper-Vallillo AJH, B.T.; Rangachari D; Kobayashi SS; Costa DB Acquired resistance to osimertinib plus savolitinib is mediated by MET-D1228 and Y1230 mutations in EGFR mutated MET amplified lung cancer. JTO Clinical and Research Reports 2020(100071) doi 10.1016/j.jtocrr.2020.100071.

44. Engstrom LD, Aranda R, Lee M, Tovar EA, Essenburg CJ, Madaj Z, et al. Glesatinib Exhibits Antitumor Activity in Lung Cancer Models and Patients Harboring MET Exon 14 Mutations and Overcomes Mutation-mediated Resistance to Type I MET Inhibitors in Nonclinical Models. Clinical cancer research : an official journal of the American Association for Cancer Research 2017;23(21):6661–72 doi 10.1158/1078-0432.CCR-17-1192. [PubMed: 28765324]

45. Mumenthaler SM, Foo J, Leder K, Choi NC, Agus DB, Pao W, et al. Evolutionary modeling of combination treatment strategies to overcome resistance to tyrosine kinase inhibitors in non-small cell lung cancer. Molecular pharmaceutics 2011;8(6):2069–79 doi 10.1021/mp200270v. [PubMed: 21995722]

46. Foo J, Michor F. Evolution of acquired resistance to anti-cancer therapy. Journal of theoretical biology 2014;355:10–20 doi 10.1016/j.jtbi.2014.02.025. [PubMed: 24681298]

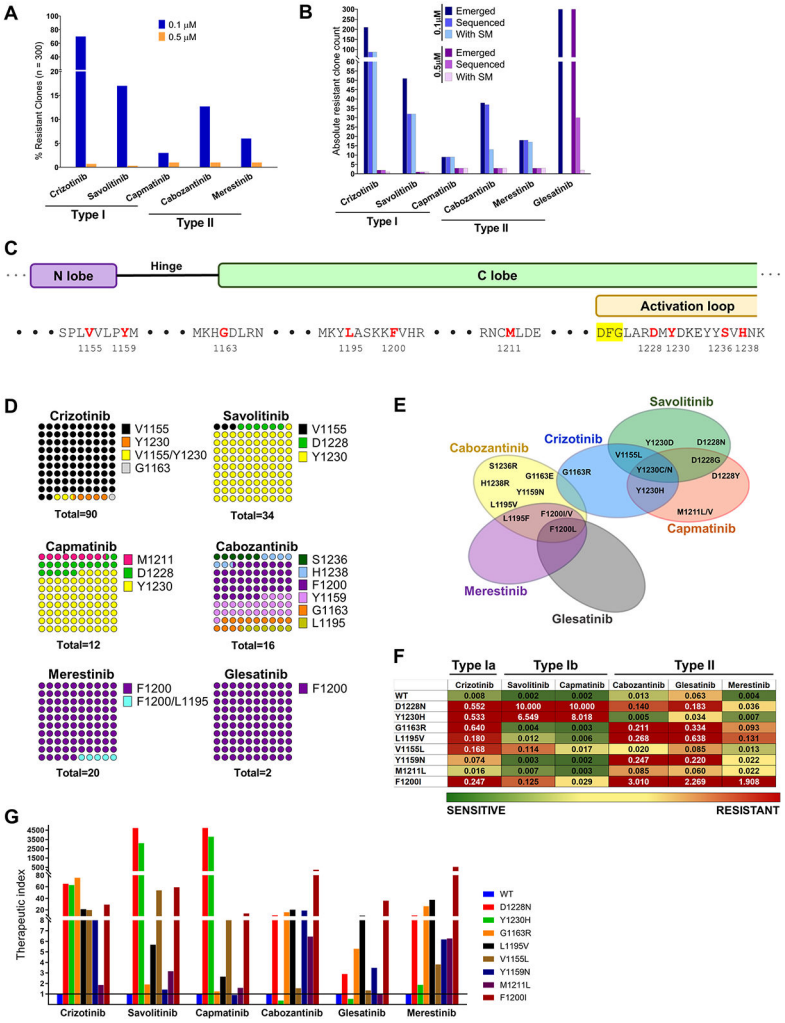

Figure 1.

Treatment with type I or II MET TKIs gives rise to distinct sets of secondary MET mutations. **A,** TPR MET Ba/F 3 cells were mutagenized with ENU and treated with MET TKIs at 0.1 or 0.5 μM in a 96 well format until resistant clones emerged. Wells with resistant outgrowth were counted and totals plotted as percentage of total seeded wells. **B,** Breakdown of number of resistant clones emerged, sequenced and ones containing a MET TKD secondary mutation (SM). **C,** Overview of the molecular position of identified resistant MET TKD mutant residues (red). **D,** DNA from randomly selected resistant clones per TKI concentration was harvested and sequenced to detect secondary mutations in the MET TKD. The distribution of mutated aa residues is given as percentages of the total number of resistant clones with an identified secondary mutation per drug treatment, combining both concentrations (n). **E,** Vann diagram illustrating the cross-resistance of each tested MET TKIs. **F,** A heat map of average IC50 values (n of ≥3) per TPR-MET Ba/F3 cell mutant and drug. Green>yellow>red denotes the spectrum of resistance from least to most resistant. The heatmap was set to a midpoint value (yellow; 20nM) of 10-times the lowest IC50 observed (2nM) and maximum value (red; 200nM) of 100-times the lowest IC50 observed. **G,** The therapeutic index of each MET TKI with respect to each MET TKD mutation is expressed

as a ratio of mutant IC50/WT IC50 per given drug. Baseline sensitivity per given drug is denoted by a line intersecting at y=1.

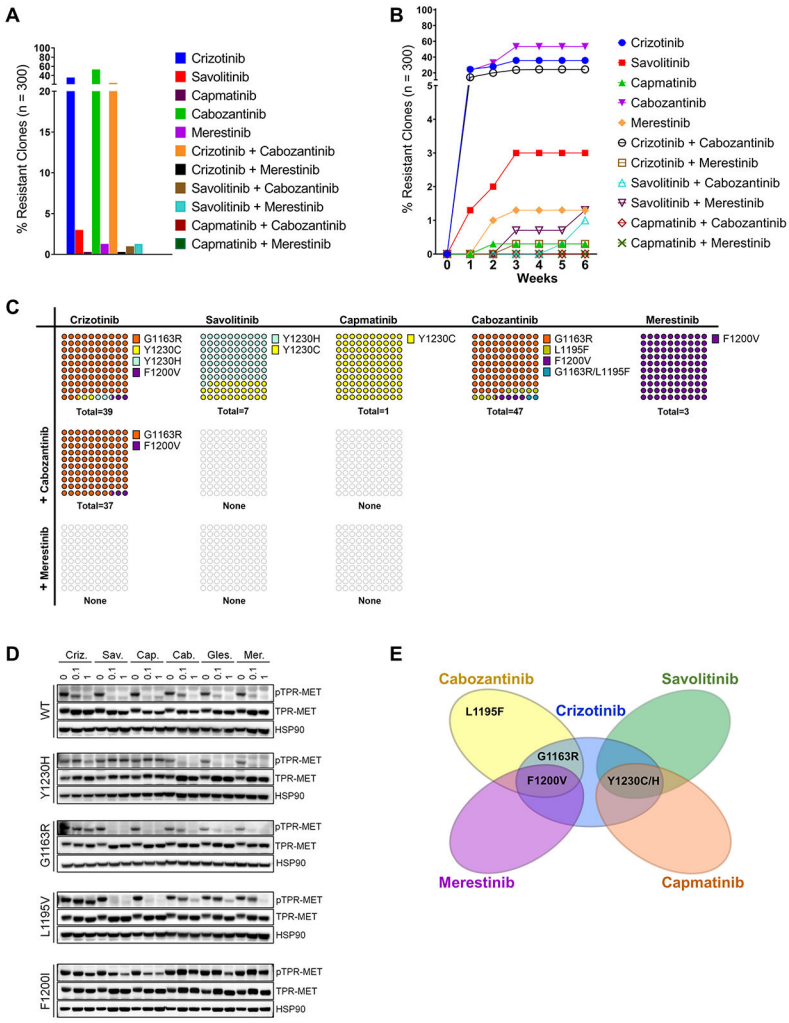

Figure 2.

Combinations of type I and II MET TKIs can prevent resistance emergence. **A,** TPR MET Ba/F 3 cells were mutagenized with ENU and treated with single agent MET TKIs at 0.3 μM or their combinations in a 96 well format until resistant clones emerged. Wells with resistant outgrowth were counted and totals plotted as percentage of total seeded wells. **B,** The latency to resistance emergence is expressed as percentages of resistance clones emerging as a function of time in weeks. **C,** DNA from randomly selected resistant clones per TKI concentration was harvested and sequenced to detect secondary mutations in the MET TKD. The distribution of secondary mutants is expressed as percentages of the total number of resistant clones with an identified secondary mutation per drug treatment (n). **D,** Western blot of TPR-MET inhibition in NIH3T3 in response to 4h treatment with each TKI at 0, 0.1 and 1uM. HSP90 is used as a loading control. **E,** Vann diagram illustrating the cross-resistance of each tested MET TKI.

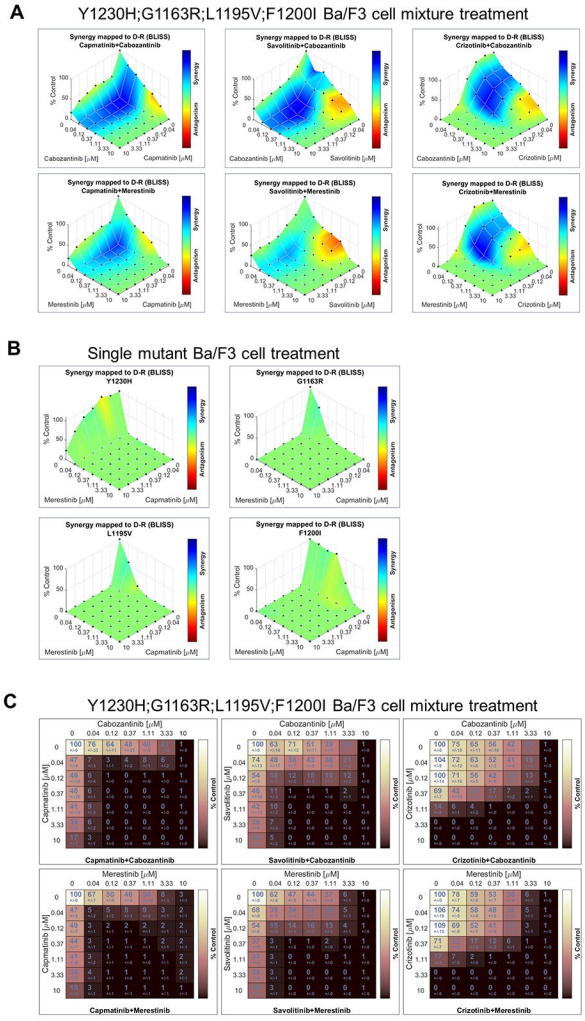

Figure 3.

Combination of capmatinib and merestinib achieve cellular synergy and highest combined dose response *in vitro*. **A,** MET TKI type I/type II combination effect on mixtures of TPR-MET mutant Ba/F3 cell lines was assessed using the Bliss independence dose-response surface model. **B,** MET TKI type I/type II combination effect on each individual TPR-MET mutant Ba/F3 cell line was assessed using the Bliss independence dose-response surface model. **C,** Matrices of combined dose response of TPR-MET mutant Ba/F3 cell line mixtures subjected to MET TKI type I/type II combination treatments, expressed in terms of viability.

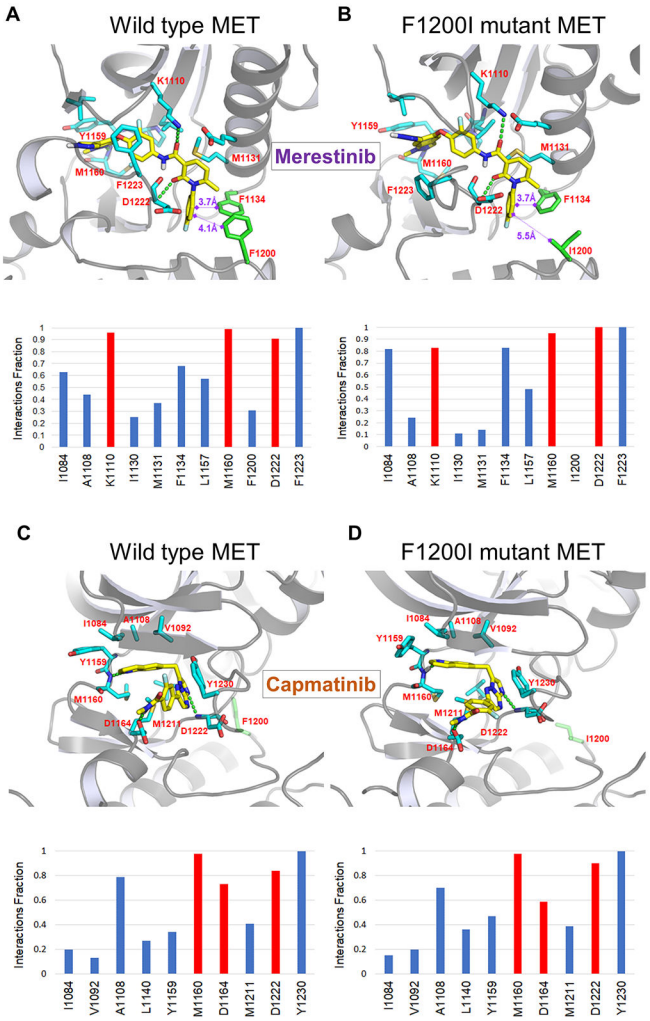

Figure 4.

A, B, Representative snapshot from the molecular dynamics (MD) trajectory of the complex of c-Met and merestinib. Merestinib is shown in yellow, interacting amino acids in cyan and the F1200 or I1200 aa residue in green. **A,** As merestinib binds to WT MET, three phenyl rings from F1134/F1200/fluorophenyl tail of merestinib form an aromatic cluster, stabilizing the interaction. Bottom panel shows protein–ligand interaction histograms for 100 ns molecular dynamic simulation of WT MET with merestinib. Red color denotes hydrogen bond interactions and blue color denotes hydrophobic interactions. **B,** The F1200I mutation destroys the aromatic cluster, weakening the merestinib-MET interaction. Bottom pane shows protein–ligand interaction histograms for 100 ns molecular dynamic simulation of MET F1200I mutant with merestinib. Red color denotes hydrogen bond interactions and blue color denotes hydrophobic interactions. The protein-ligand interaction at I1200 is fully abolished. **C, D,** Representative snapshot from the molecular dynamics (MD) trajectory of the complex of MET and capmatinib. Capmatinib is shown in yellow, interacting amino acids in cyan and the F1200 or I1200 aa residue in green. **C,** As capmatinib binds to the WT MET, π-π stacking with Y1230 in the activation loop forms, stabilizing the interaction. Bottom panel shows protein–ligand interaction histograms for 100 ns molecular dynamic

simulation of WT MET with capmatinib. Red color denotes hydrogen bond interactions and blue color denotes hydrophobic interactions. **D,** Capmatinib keeps an effective π-π stacking interaction with Y1230 in MET F1200I mutant c-Met mutant. Bottom panel shows protein–ligand interaction histograms for 100 ns molecular dynamic simulation of MET F1200I with capmatinib. Capmatinib exhibits an efficient binding interaction with the mutant. Red color denotes hydrogen bond interactions and blue color denotes hydrophobic interactions.

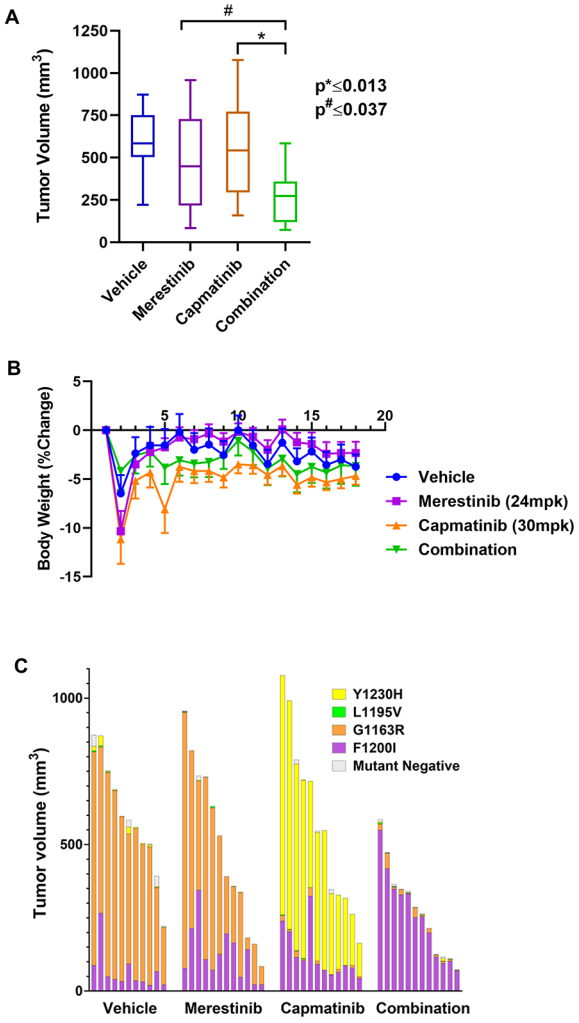

Figure 5.

The merestinib/capmatinib combination shows efficacy and tolerability *in vivo*. **A,** A box plot of volume of tumors harvested from mice on day 18 of treatment. *, # denote significance. **B,** Plot of body weight percent change of treated mice as a function of treatment time. **C,** The individual contribution of each TPR-MET mutant was determined by ddPCR at the end of the study and expressed as percent tumor volume. Each bar represents an individual treatment subject.

Table 1.

Day 18 *in vivo* drug synergy

SF ratio *	1.46
Synergy (%)	46
T-statistic	1.86
One-sided p value	0.038

* Ratio of surviving fraction under Bliss independence to surviving fraction of the capmatinib/merestinib combination on day 18